ORIGINAL ARTICLE

Prediction and optimization kerf width in laser beam machining of titanium alloy using genetic algorithm tuned adaptive neuro-fuzzy inference system

Min Ji[1] · Muthuramalingam Thangaraj[2,3] · Saravanakumar Devaraj[4] · Ryszard Machnik[3] · Nikolaos E. Karkalos[5] · Panagiotis Karmiris-Obratański[3,5]

Abstract

In the power diode laser beam machining (DLBM) process, the kerf width (K_W) and surface roughness (SR) are important factors in evaluating the cutting quality of the machined specimens. Apart from determining the influence of process parameters on these factors, it is also very important to adopt multi-response optimization approaches for them, in order to achieve better processing of specimens, especially for hard-to-cut materials. In this investigation, adaptive neuro-fuzzy inference system (ANFIS) and genetic algorithm tuned ANFIS (GA-ANFIS) were used to predict the K_W on a titanium alloy workpiece during DLBM. Five machining process factors, namely power diode, standoff distance, feed rate, duty cycle, and frequency, were used for the development of the model due to their correlation with K_W. As in some cases, traditional soft computing methods cannot achieve high accuracy; in this investigation, an endeavor was made to introduce the GA-assisted ANFIS technique to predict kerf width while machining grooves in a titanium alloy workpiece using the DLBM process based on experimental results of a total of 50 combinations of the process parameters. It was observed that FIS was tuned well using the ANN in the ANFIS model with an R^2 value of 0.99 for the training data but only 0.94 value for the testing dataset. The predicting performance of the GA-ANFIS model was better with less value for error parameters (MSE, RMSE, MAE) and a higher R^2 value of 0.98 across different folds. Comparison with other state-of-the-art models further indicated the superiority of the GA-ANFIS predictive model, as its performance was superior in terms of all metrics. Finally, the optimal process parameters for minimum K_W and SR, from gray relational–based (GRB) multi-response optimization (MRO) approach, were found as 20 W (level 2) for laser power, 22 mm (level 5) for standoff distance, 300 mm/min (level 5) for feed rate, 85% (level 5) for duty cycle, and 18 kHz (level 3) for frequency.

Keywords ANFIS · GA-ANFIS · Titanium · Kerf width · Prediction · DLBM · Optimization

✉ Panagiotis Karmiris-Obratański
karmiris@agh.edu.pl; pkarm@mail.ntua.gr

1 School of Computer Science, Xijing University, Xi'an 710123, Shaanxi, China

2 Department of Mechatronics Engineering, SRM Institute of Science and Technology, SRM Nagar, Kattankulathur 603203, Chengalpattu District, Tamil Nadu, India

3 Advanced Manufacturing Laboratory, Department of Manufacturing Systems, Faculty of Mechanical Engineering and Robotics, AGH University of Krakow, Krakow 30-059, Poland

4 School of Mechanical Engineering, Vellore Institute of Technology, Chennai 600127, India

5 Laboratory of Manufacturing Technology, School of Mechanical Engineering, National Technical University of Athens, Athens 157 80, Greece

1 1. Introduction

The accelerated progression of technological advancements, coupled with the rising demand for superior products and novel materials, has culminated in the evolution and refinement of production methodologies [1]. Although conventional machining processes such as turning, milling, and drilling were used for over a century in various demanding tasks in the manufacturing industry and many advancements, such as the use of advanced coolants and cooling methods, the use of specially designed tools or assistive technologies has been developed in order to alleviate some of the common issues restricting the high performance of these processes such as tool wear, machining chatter and chip control, improvement of their efficiency is still limited. Especially, non-conventional processes have shown to be especially suited for efficient machining of difficult-to-cut materials, including hardened steels, titanium alloys, and nickel superalloys as well as ceramics and composite materials. A particularly interesting non-conventional method is laser beam machining (LBM), which is a cutting-edge manufacturing process that employs a high-energy laser beam to sculpt materials with intricate precision, often dealing with variables that are nonlinear, imprecise, and multifaceted in nature [2]. Due to its non-conventional nature, LBM does not require physical contact between the workpiece and the tool, reducing the need for expensive and complex tooling for the machining setup and also eliminating the drawback of cutting tool wear during conventional machining processes [3].

LBM is a sophisticated subtractive manufacturing technique, whose efficacy is governed by intricate interrelationships among several key parameters, relevant to both the machine tool employed and the workpiece material, namely laser power, laser beam spot size, feed rate, use of assisting gas, thermo-mechanical properties of the workpiece, etc [4]. The laser's power dictates the energy intensity imparted, while its pulse duration and frequency modulate the temporal distribution of this energy [5, 6]. Spot size, derived from the focal length of the employed lens, determines the spatial concentration of the laser beam, influencing the resolution and precision of machining [7, 8]. The feed rate represents a balance between achieving desired material removal rates and minimizing thermal effects [9]. Assisting gases not only influence the ejection of molten material but can also chemically interact with the workpiece, affecting surface characteristics [10]. Material-specific properties, such as thermal conductivity and reflectivity, play pivotal roles in the beam-material interaction dynamics [11]. Ambient conditions, particularly temperature and humidity, might subtly influence beam propagation and absorption. Understanding and calibrating these parameters, in harmony, are paramount for ensuring optimal, reproducible, and scientifically consistent results in LBM applications [12].

Based on the mentioned above complex LBM physical phenomena, an optimization of these parameters is crucial to increase the precision and minimize the energy and materials waste [7, 13]. Apart from experimental work and statistical analysis of the findings based on methods such as ANOVA, addressing the complexities inherent in this process requires advanced computational tools, and this is where the Adaptive neuro-fuzzy inference systems (ANFIS) comes into play [14]. ANFIS, an innovative model that blends the adaptive capabilities of artificial neural networks (ANN) [15] with the logical reasoning of fuzzy inference systems (FIS) [16], is uniquely poised to understand and model the nuanced parameters of LBM. By exploiting the individual strengths of ANN and FIS, ANFIS offers a compelling strategy for function approximation and system modeling, especially relevant in the dynamic world of laser manufacturing. From an engineering viewpoint, the brilliance of ANFIS resides in its adeptness at navigating the challenging terrains of nonlinearities and imprecisions, thereby paving the way for more accurate and efficient laser machining outcomes [17].

The efficacy of LBM is deeply contingent upon its input parameters, and for this purpose many researchers have conducted comprehensive experimental and numerical studies in order to determine the correlation between these parameters and some of the outcomes of LBM. It is widely accepted that a paramount machining performance metric is surface roughness [18]. To delineate the correlation between surface quality and these parameters in LBM drilling, Muthuramalingam et al. [19] undertook an optimization study on a titanium grade 5 alloy utilizing a CO_2 laser. Through the Taguchi gray relationship analysis (GRA), it was discerned that the laser power (LP) and stand-off distance (SoD) significantly influence the surface roughness (SR) [19]. Specifically, a higher LP combined with a reduced SoD results in a diminished SR. Chatterjee et al. [20] in their study used artificial intelligence techniques to predict the quality characteristics of Ti6Al4V and AISI 316 after laser hole drilling. From the analytical evaluation, it is discerned that the Multi Gene Genetic Programming (MGGP) model exhibits a diminished root mean square error (RMSE) relative to the ANFIS model when evaluating performance metrics. This data suggests that MGGP holds a heightened potentiality and robustness in prognosticating the performance parameters associated with the laser beam micro-drilling operation. Conclusively, the MGGP models manifest superior prediction fidelity in juxtaposition with the ANFIS model. Numerous researchers have endeavored to devise an AI algorithm tailored for predicting and optimizing process outcome such as material removal rate (MRR) and kerf width in LBM,

especially given that a reduced kerf width is integral to ensuring optimal cut quality [21].

Campanell et al. [22] used an ANN model to identify the values of scan speed and pulse frequency that correlate with a predetermined depth of MRR, thereby enhancing the efficiency of the process of laser milling. The results show that there is an inverse relationship where scanning speed (V) decreases with a rise in the ablation depth. Ablation depths below 2.5 μm correspond with higher velocities, approaching the upper limit of 2000 mm/s considered in this study. Conversely, greater ablation depths exceeding 10 μm align with scan speeds in the 460 to 510 mm/s range. Rajamaniaet al. [23] performed an ANFIS modelling and whale optimization algorithm to predict the MRR, kerf taper angle, and SR during a fiber laser cutting of Hastelloy C276. The results show that ANFIS model, having the least prediction errors, is more efficient than the multiple linear regression models approach. Whale optimization algorithm proves to be the best method for optimizing the LBC process, with optimal parameters being 3 bar of gas pressure, 319.8 mm/min cutting speed, 5.93 J pulse energy, and 2.97 mm stand-off distance. Finally, Bakhtiyari et al. [24] employed ANN and ANFIS algorithms to represent the cadmium plasma attributes under conditions of local thermodynamic equilibrium during laser ablation. The study results indicate that the suggested machine learning algorithms proficiently create precise models to forecast the temporal and spatial changes of the laser-induced plasma (LIP). The need of implementing the diode-based LBM (DLBM) process is increasing predominantly [25]. The higher laser-power diode can increase the plasma energy developed across the machining zone [26].

Apart from surface quality and MRR, the kerf width (K_W) is also an important quality metric on accessing the cutting quality of LBM process, as it indicates not only the material wastage but also the cutting dimensional accuracy [27]. More specifically, Löhr et al. [28] performed a comprehensive analysis of the deviations of the kerf profile during CO_2 laser processing of PMMA workpieces, showing also that focal point position, cutting speed, and laser power are the most important parameters regarding kerf width. Pramanik et al. [29] investigated the effect of various parameters, including sawing angle, laser power, duty cycle, pulse frequency, and scanning speed on the kerf quality during fiber laser micro-machining of Ti-6Al-4 V. Comparable results on the effect of process parameters on kerf quality were also obtained in another study by the same authors on stainless steel workpieces, who analyzed also the kerf taper angle [30]. Analysis of experimental data indicated that all parameters were statistically significant but pulse frequency, duty cycle, and scanning speed were the most important. Son and Lee [31] correlated the kerf width with volume energy during LBM and found that higher kerf widths are produced under higher volume energy and that laser power

has a more significant effect on kerf width than cutting speed. Naskar et al. [32] conducted experiments on LBM of aluminum alloy 7075 and analyzed the effect of laser power, pulse frequency, and assist gas pressure on kerf width and heat-affected zone (HAZ). It was found that all parameters were important and that kerf width is minimized at low laser power due to less thermal energy incorporation, moderate assist gas pressure, and higher pulse frequency.

Bakhtiyari et al. [7] analyzed comprehensively the influence of several parameters during LBM, underlined the importance of kerf width as a quality indicator, and mentioned that high laser power leads to increase of kerf width as well as waviness of the produced profiles whereas increased cutting speed reduces the kerf width. Genna et al. [33] conducted experiments under five different parameters, such as workpiece thickness, feed rate, assist gas pressure, and focus position, and argued that increased cutting speed reduces kerf width due to the reduced irradiation time and lower energy but the increase of kerf width observed in some cases can be attributed to the change in cut front inclination. Lind et al. [34] studied the effect of beam shape on kerf geometry during LBM and developed a model for determining the maximum possible cutting speed depending on the geometry of kerf. Kusuma and Huang [35] conducted a comprehensive comparison of different soft computing models for kerf width prediction during LBM, showing that a random forest model was able to achieve the lowest MAPE in both training and testing. Khoshaim et al. [36] performed laser machining experiments on PMMA sheets and found out that kerf deviation was mostly affected by workpiece thickness and cutting speed. Increased cutting speed as well as gas pressure and laser power increased the achieved kerf width [37, 38].

Even though several research efforts were performed on the prediction of LBM process quality metrics, only less research attention was provided on enhancing the process of the diode-based LBM, and also few amounts of attention were given to the prediction of K_W during the machining process by appropriate soft computing models [39]. As K_W indicates the overcut made during the cutting process and indirectly represents materials wastage that happened during the machining process [40], apart from reducing the surface roughness, it is essential to reduce K_W as much as possible due to the high cost of titanium alloy specimens. Hence, it needs to be predicted before the machining process for choosing the optimal process parameters. Moreover, it is important that the influence of the DLBM process factors on K_W and surface roughness has to be investigated for achieving better quality during diode laser machining. Thus, in the present work, a comprehensive experimental work based on Taguchi orthogonal array design is conducted in order to investigate the influence of process parameters on kerf width and surface roughness of DLBM processed specimens at first and then, an ANFIS-based predictive model and a GA-ANFIS model

for K_W obtained during DLBM were developed based on the experimental data and evaluated regarding their capabilities, in comparison with other established methods, such as regression methods and regression tree models. Finally, an optimization procedure by the gray relational–based (GRB) multi-response optimization method was carried out in order to determine the optimum conditions for obtaining the highest quality of the produced features based on the minimization of both kerf width and surface roughness values.

2 Experimental methodology

In this work, the effect of using advanced AI methods for the prediction of kerf quality during laser machining of titanium alloy is investigated, along with the determination of optimum process parameters values which can lead to reduced kerf width and surface roughness. A comprehensive experimental work is conducted, taking into account five different process parameters under multiple levels each and then the correlation of these parameters with kerf width and surface roughness is determined. In order to improve the precision and robustness of the prediction of kerf width, apart from the usually developed regression models, several AI models, namely decision trees (DT), adaptive neuro-fuzzy inference system (ANFIS), and a hybrid genetic algorithm - adaptive neuro-fuzzy inference system (GA-ANFIS) model, are developed and compared based on multiple metrics in order to determine the most preferable approach for the specific problem. Moreover, the hybrid GA-ANFIS model is compared to other state-of-the-art models such as support vector machine (SVM), multilayer perceptron neural network, Gaussian process regression, and kernel regression in order to further prove the superiority of this method. Finally, a gray relational–based optimization method is employed in order to provide the parameter combination which leads to minimum kerf width and surface roughness values.
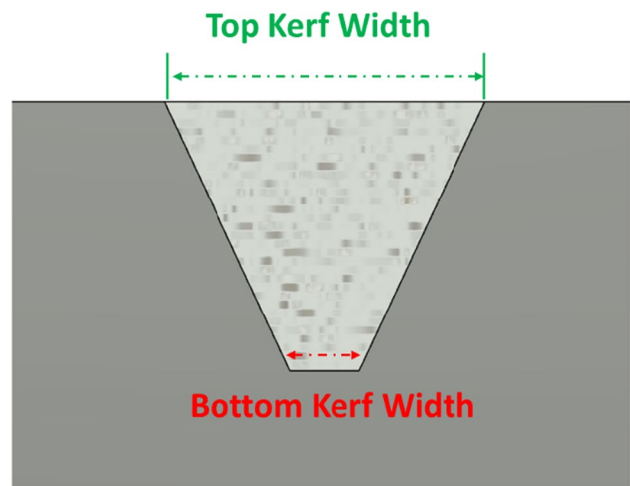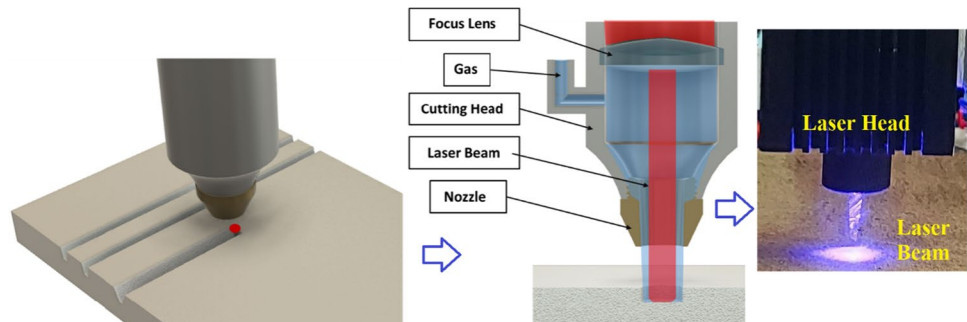

Fig. 2 Schematic diagram of top and bottom kerf widths in a section of a cut created by LBM

2.1 Experimental design

The aerospace and industrial sectors make extensive use of titanium (Ti-6Al-4 V) alloy. Thus, due to its frequent use in demanding applications, it was chosen for the current study. In this study, the milling process was performed over the workpiece specimens using a customized power diode-assisted laser beam machining process (DLBM) process [41]. The power supply unit (PSU) of 12 V has been connected to the laser power module, which has an input electrical power of 10 W and 20 W with a laser driver module for controlling the laser beam [42]. The process parameters in the DLBM process such as standoff distance (SOD), feed rate (FR), duty cycle (DC), and frequency (F) along with powder diode (PD) were selected to examine their effects on the thickness of the K_W [27]. The range of process variable settings for process factors was chosen as indicated in Table 1. Figure 1 shows the graphical representation of the laser milling.

Kerf width (K_W) is the removed material width during the machining process, indicated in the schematic diagram of Fig. 2. Celestron's digital microscope software

Fig. 1 Graphical representation of the laser milling process

Table 1 Process factors in the DLBM study

Process factors notation	Process variables	Unit
PD	10, 20	W
SOD	18, 19, 20, 21, 22	mm
FR	200, 225, 250, 275, 300	mm/min
DC	65, 70, 75, 80, 85	%
F	16, 17, 18, 19, 20	kHz

was utilized to acquire images and to measure the kerf width. The proposed study used a USB digital microscope to measure the kerf width of machined specimens. The digital microscope was set to a magnification of 52.834% to capture the top surface of the titanium workpiece. In this experiment, the kerf width was measured based on ten different positions for each test, using the ruler function in Celestron Micro Capture Pro. The ruler was first calibrated with a Vernier scale to ensure accuracy, and the ten sample measurements were then averaged to determine the kerf width of each sample. The surface roughness of the cut surface was quantitatively measured using an Alicona Infinite focus microscope by setting up lambda filter (cutoff wavelength) on 80 μm. Each machining trial was replicated two times to enhance the measurement accuracy and all the performance characteristic values used for analysis were obtained from computing the mean values of the repeated trials. The surface roughness was measured from scanned areas at the center of the machined surface.

By using an experimental design based on L_{25} Taguchi orthogonal array for four parameters under five levels and duplicating the design twice, as laser power was varied at two levels, 50 different experimental training combinations were carried out in total. The number of levels for the different variables was determined by analyzing the literature and discussing with laser machining experts in this field. Especially regarding laser power, it was observed that the suggested two laser power values can be related to the limiting values for obtaining optimal values for the process. Moreover, the choice of laser power depends on the hardware requirements and commercially availability for diodes used for the same process. This approach not only allows a very comprehensive evaluation of the effect of each parameter on kerf width during laser machining of titanium alloy but also maintains a relatively low required time and cost for the experiments.

2.2 Fuzzy inference system (FIS)–based prediction approach

A fuzzy inference system (FIS) is a type of artificial intelligence model that operates based on fuzzy logic. Fuzzy logic is a mathematical framework that deals with uncertainty and imprecision, allowing for the representation and manipulation of vague and uncertain information. It is particularly useful in situations where conventional binary logic (true/false) for decision making may not be suitable.

The fuzzy inference system consists of four main components:

Fuzzification This step involves converting crisp (exact) input data into fuzzy sets. Fuzzy sets are characterized by membership functions that assign a degree of membership to each element of the set. These membership functions define the degree of similarity between the input data and the fuzzy sets.

Fuzzy rule base The fuzzy rule base contains a set of IF-THEN rules that express the relationship between the fuzzy inputs and fuzzy outputs. Each rule consists of a condition (antecedent) and a conclusion (consequent) linked by linguistic terms. The condition part uses the fuzzy sets obtained from the fuzzification step, and the conclusion part defines the fuzzy sets that represent the desired output.

Inference engine The inference engine evaluates the fuzzy rules based on the fuzzy input values to determine the corresponding fuzzy outputs. The degree of activation of each rule is determined by the membership values of the input data in the respective fuzzy sets.

Defuzzification In many applications, the fuzzy output needs to be converted back into crisp values. Defuzzification is the process of aggregating the fuzzy outputs and obtaining a single crisp output value. Various methods can be used for defuzzification, such as centroid, mean of maximum, or weighted average.

Tuning a fuzzy inference system (FIS) involves adjusting its parameters and rules to optimize its performance for a specific task or application. Proper tuning is essential to ensure that the FIS can accurately model the underlying system, make accurate predictions, or control a process effectively [43]. There are several techniques for tuning a FIS, depending on the type of FIS and the nature of the problem at hand [44]. There are various algorithms and optimization techniques that can be used for tuning fuzzy inference systems. Some of the common ones are grid search, genetic algorithms, particle swarm optimization (PSO), simulated annealing, differential evolution, ant colony optimization (ACO), and particle competition and cooperation optimization (PCCO). The process of tuning involves evolutionary learning to solve the optimization problem as shown in Fig. 3.

Fig. 3 Tuning process of the fuzzy inference system
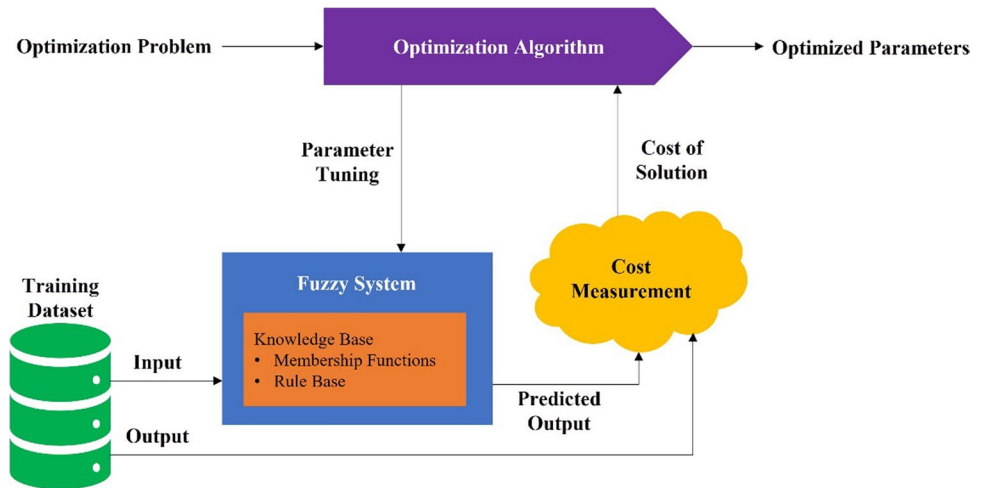
2.3 Adaptive neuro-fuzzy inference system (ANFIS)

ANFIS is a hybrid computational model that combines the capabilities of artificial neural networks (ANNs) and fuzzy logic to perform inference and learning tasks [13]. Fuzzy logic systems use fuzzy sets and rule base for inferring output parameters based on input data. Development of the rule base and structure of fuzzy systems requires an expert knowledge about the system. The fuzzy rules are defined based on linguistic variables and membership functions, which determine the degree of membership of input variables to different fuzzy sets. An artificial neural network (ANN) is used to approximate the consequent part of fuzzy rules. The ANN is responsible for tuning the parameters (weights and biases) of the nodes in the output layer, which correspond to the consequent part of the fuzzy rules. ANFIS was developed as a tool for modelling and predicting complex systems based on input-output data [45].

The architecture of an ANFIS typically consists of several layers as shown in Fig. 4, each performing specific functions in the modelling and inference process [46, 47]. The functions of different layers in ANFIS are listed below.

Input layer The input layer receives the crisp input variables or data. Each input node represents an input variable.

Membership function layer The membership function layer fuzzifies the crisp input data into fuzzy linguistic variables. Each node in this layer represents a membership function associated with a specific input variable. Membership functions define the degree of membership of an input value to a particular fuzzy set.

Normalization layer The normalization layer computes the normalized firing strength of each rule. It takes the fuzzy membership degrees from the membership function layer as inputs and normalizes them.

Rule layer The rule layer computes the firing strength (activation level) of each rule. It combines the normalized membership degrees from the normalization layer based on the fuzzy rules. Each node in this layer represents a specific rule.

Aggregation layer The aggregation layer aggregates the outputs of the rules. It combines the outputs of the rule layer using the firing strengths obtained in the previous layer.

Output layer The output layer provides the final output of the ANFIS model. It takes the aggregated outputs from the aggregation layer and performs defuzzification to convert the aggregated output into a crisp value.

Parameter learning The most important feature of the ANFIS algorithm is its ability to adjust the parameters (weights and biases) of the network to optimize the output. Forward Pass Perform is a forward pass through the network, passing the input data through the fuzzy inference system. It computes the outputs of each node based on the fuzzy rules and membership functions. Error calculation compares the computed outputs with the desired outputs and calculate the error. Backward Pass (gradient calculation) propagates the error back through the network and calculates the gradients of the error with respect to the parameters. Parameters such as weights and biases are updated using an optimization algorithm (e.g., gradient descent) to minimize the error. This process iterates for a specified number of iterations or until convergence. It allows the ANFIS model to adjust its parameters and improve its performance on the training data.
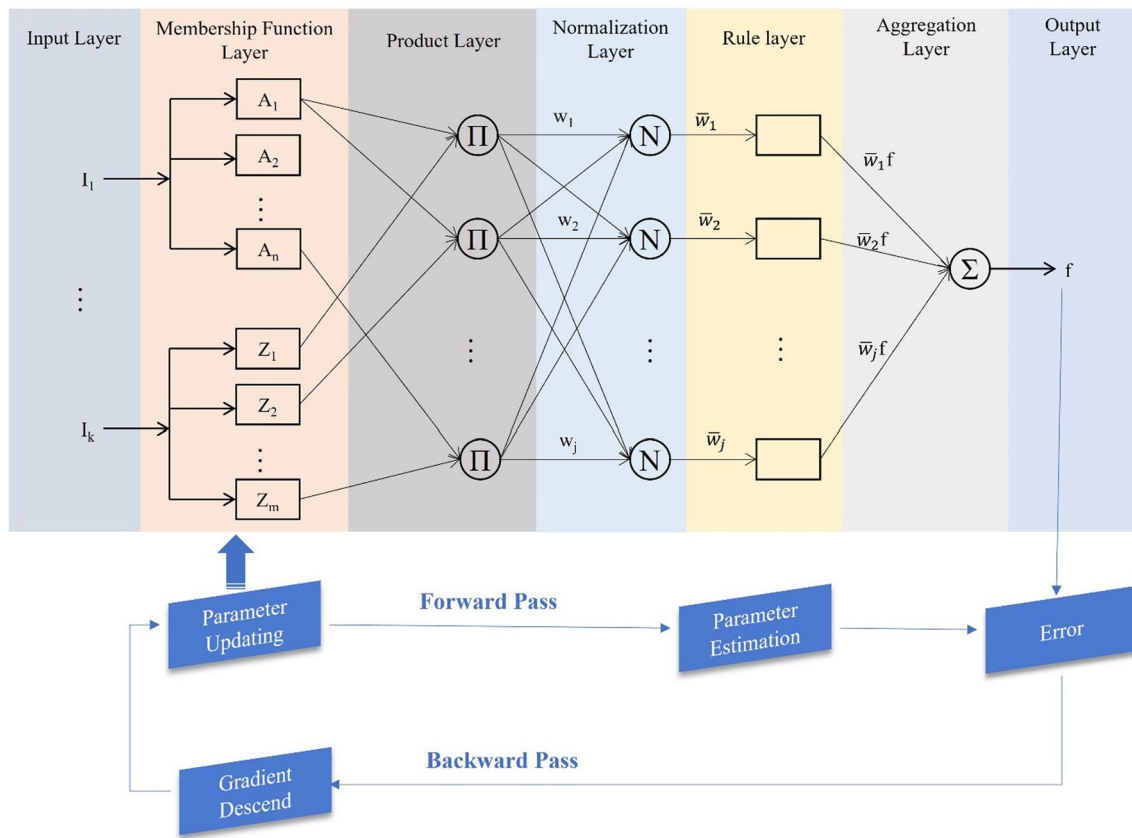
Fig. 4 ANFIS architecture and learning process

2.4 Genetic algorithm tuned adaptive neuro-fuzzy inference system (GA-ANFIS)

Genetic algorithm (GA) is a heuristic search and optimization algorithm inspired by the process of natural selection and genetics in biology. The basic idea behind a GA is to start with a population of possible solutions to a problem, and then use a process of selection, crossover, and mutation to generate new solutions that may be better than the previous ones. The solutions are encoded as chromosomes, which are strings of binary or real-valued numbers that represent potential solutions to the problem. The key advantages of GA are that it can handle a wide range of problems and search spaces, and it can work in parallel to generate multiple solutions simultaneously.

Genetic algorithm-tuned ANFIS is a hybrid machine learning approach that combines the ANFIS with GA optimization to improve the performance of ANFIS as shown in Fig. 5. In a GA-tuned ANFIS approach, the GA algorithm is used to optimize the parameters of the ANFIS model, such as the membership functions and the scaling factors, to improve the accuracy of the model [48]. The GA algorithm searches for the optimal set of parameters by evaluating the fitness of different parameter sets using a fitness function, which is typically the mean squared error between the predicted and

actual values. The advantage of using GA-tuned ANFIS is that it can improve the accuracy of ANFIS by optimizing the parameters more efficiently than traditional trial-and-error methods. It can also handle complex and non-linear systems, and adapt to changing environments [49].

2.5 *K*-fold cross-validation

K-fold cross-validation is a technique used in machine learning to evaluate the performance of a model. In this method, the dataset is divided into *K* equal-sized partitions, or "folds." The model is then trained *K* times, each time using $K-1$ folds for training and one fold for testing. For example, if we choose $K = 5$, the data would be split into five folds, each containing one-fifth of the data. The model would be trained five times, each time using a different fold as the test set and the remaining four folds as the training set. The results from each of the five tests are then averaged to produce a final evaluation metric, such as accuracy or error rate [50].

The advantage of using *K*-fold cross-validation is that it provides a more accurate estimate of the model's performance than simply splitting the data into a single training and testing set. By using multiple folds, we are able to train and test the model on different parts of the dataset, which can help to reduce the impact

Fig. 5 Structure of genetic algorithm–tuned ANFIS system
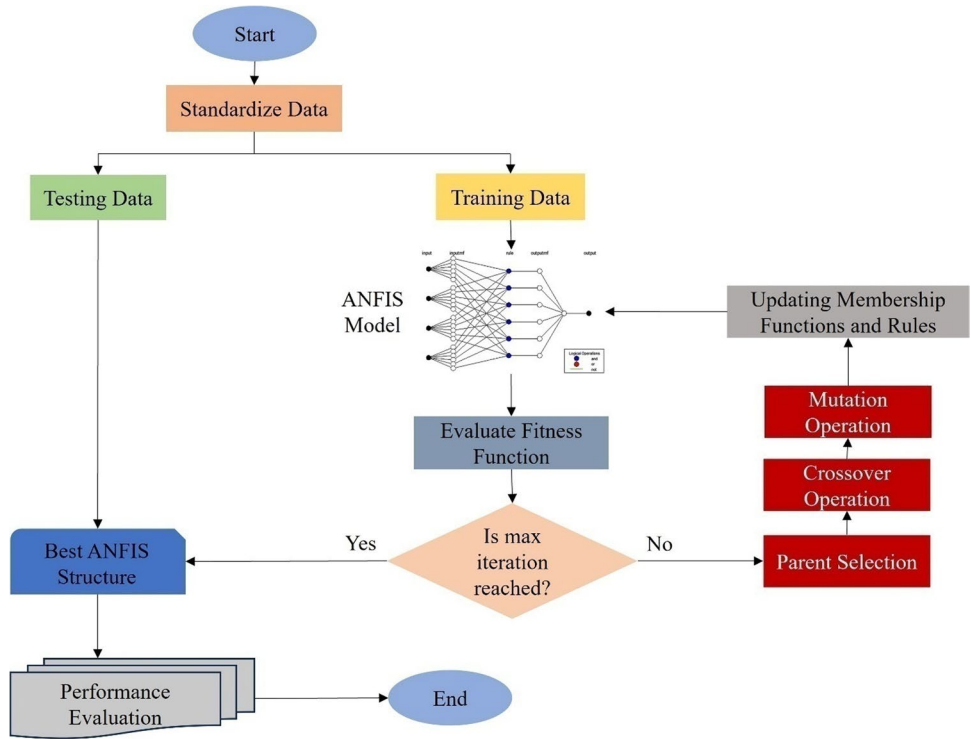
of any particular subset of the data having an unusual distribution. Another advantage of *K*-fold cross-validation is that it allows us to make better use of our limited dataset, particularly when the amount of data available for training is small. By repeatedly training the model on different parts of the dataset, it is possible to get a better estimate of the model's true performance [51].

Finally, it is necessary to note that the performance of the predictive models is evaluated using several standard performance measures as listed below.

Mean squared error (MSE) This is one of the most common measures used to evaluate the accuracy of regression models. It calculates the average squared difference between the predicted values and the actual target values. MSE is given as follows:

$$MSE = \frac{1}{n} \sum_{i=1}^{n} \left(y_m - y_p\right)^2 \tag{1}$$

where *n* is number of data samples, and y_m is the experimental value, while y_p is the predicted value.

Root mean squared error (RMSE) RMSE is the square root of the MSE. It provides a measure of the typical prediction error and is often preferred when the errors have significant magnitude variations. RMSE is given as follows:

$$RMSE = \sqrt{\frac{1}{n} \sum_{i=1}^{n} \left(y_m - y_p\right)^2} \tag{2}$$

Mean absolute error (MAE) MAE is another measure of the prediction error, but it takes the absolute difference between predicted and actual values. It is less sensitive to outliers than MSE.

$$MAE = \frac{1}{n} \sum_{i=1}^{n} \left|y_m - y_p\right| \tag{3}$$

R-squared (R²) *R*-squared measures the proportion of variance in the target variable that is predictable from the input variables. It provides an indication of how well the model fits the data, with values ranging from 0 to 1. Higher *R*-squared values indicate a better fit.

$$R^2 = \frac{\left[\sum_{i=1}^{n} \left(y_m - \bar{y_m}\right)^2\right] - \left[\sum_{i=1}^{n} \left(y_m - y_p\right)^2\right]}{\left[\sum_{i=1}^{n} \left(y_m - \bar{y_m}\right)^2\right]} \tag{4}$$

3 Results and discussion

3.1 Analysis and discussion of the experimental results

By using an experimental design based on Taguchi L_{25} orthogonal array for four parameters under five levels

and performing the same experiments with two different levels of laser power, 50 different experimental training combinations were carried out in total, as can be seen in Table 2. The typical K_W and surface roughness (Ra) values presented in Table 2 were then thoroughly analyzed based on statistical methods in subsections 3.1.1 and 3.1.2 respectively.

3.1.1 Analysis of kerf width values

At first, as can be seen from Table 2, a considerable amount of experimental tests has been carried out in this work, by varying the values of five process parameters within an appropriate range, relevant to the practical conditions often selected for this process. Furthermore, by observing the results of Table 2, it becomes obvious that the values of kerf width vary considerably within the range of different process parameters chosen for the experiment. More specifically, values as low as 0.46 mm up to 2.1019 mm were recorded under different conditions, indicating that the experimental investigation was comprehensive enough, as it was able to capture different probable cases of material removal during DLBM.

Thus, based on the analysis of the experimental results, the main effects plot regarding kerf width can be observed in Fig. 6. At first, it can be clearly observed that the largest variation occurs for the laser power even though its values vary in the range of 10–20 W, as it can induce a considerable variation of the produced kerf width. Furthermore, feed rate has also a noticeable impact on the kerf width as well as duty cycle, to a slightly lesser extent, whereas standoff distance (SOD) and frequency have a less pronounced effect on the variation of kerf dimension. In the case of laser power (LP), feed rate (FR), duty cycle (DC), and SOD, a clear increasing trend can be observed as the values of these parameters increase, implying that it is not favorable to use high values of these parameters when the main objective of the investigation is to achieve low kerf width, although some of these parameters are expected to increase the MRR. On the other hand, frequency exhibits a more complex trend by initially increasing kerf width, then decreasing its values and finally reaching a moderate value at the highest frequency.

The observed trends can be explained based on the mechanics of material removal during laser machining of titanium alloy. Increased laser power contributes to a higher amount of heat being introduced to the workpiece during LBM; thus, it is expected that the zone of melting and evaporation, as well as the HAZ, will be larger when a higher laser power is used. This is evident from most of the experimental works in the relevant literature and was particularly noted in the work of Son and Lee [33], who particularly correlated volume energy and kerf dimensions. The increase of kerf width by increase of SOD can be explained due to the changes in the focusing of the beam as well as energy distribution when it acts from different distances. At higher standoff distances, the divergence of the beam becomes higher, with the spot size being slightly increased. Thus, HAZ and material removal increase, with a wider kerf width developing.

Moreover, the trend between the cutting speed and the kerf width was found to be almost a linearly increasing one. In general, a higher feed rate is related to a shorter time of interaction between the laser beam and the workpiece, so a lower amount of energy is transmitted to the workpiece [52]. Thus, the increased amount of heat is not sufficient to evaporate or not even melt a considerable amount of material around the irradiated region, resulting in less material removal and narrower top kerf width, whereas also taper increases due to the increased lag and larger difference between the size of top and bottom kerf width. However, in a few cases where relatively high cutting speeds were used, it was shown that the use of higher feed rate can lead to higher kerf widths [53]. This phenomenon was observed by Rao et al. in sheet machining and was attributed to higher vibrations observed in the direction perpendicular to the cutting direction. A non-linear correlation of cutting speed and kerf width at different ranges of cutting speed was also noted by Darwish et al. [54] and Kondayya and Krishna [55]. A plausible explanation is relevant to the possibility of a "self-focusing" or "self-induced absorption" phenomenon due to variations in cut front formation [33], which can be caused especially by the formation of a dense and turbulent plume which leads to higher absorption [56] and eventually enlarges the kerf width. Moreover, this phenomenon can be relevant to the material properties of titanium workpiece, such as low thermal conductivity or higher thermal expansion coefficient leading to lower heat dissipation, higher heat accumulation, and material distortion.

The duty factor is relevant to the ratio of the time the laser is operating to the total cycle time, implying that for higher values, the laser is operating for the larger percentage of the cycle. Thus, higher values of duty factor can be directly correlated with larger kerf width, as more energy is delivered to the workpiece, leading to more intense melting and vaporization; thus, more energy is available to melt the top surface of the kerf [29, 57]. Moreover, the pulse frequency is related to the number of laser pulses per unit time, so that higher frequency is related to smaller exposure time for each pulse and results in a narrower kerf width but also less uniform [29], as it was observed for frequencies over 18 kHz in the present study.

Regarding the relative importance and significance of process parameters, analysis of variance (ANOVA) was performed on the experimental data, as can be seen in Table 3. Every parameter, except from pulse frequency,

Table 2 Experimental results

Experiment number	Laser power (W)	Standoff distance (mm)	Feed rate (mm/min)	Duty cycle (%)	Frequency (kHz)	Kerf width (mm)	Surface roughness (μm)
1.	10	18	200	65	16	0.4680	0.524
2.	10	18	225	70	17	0.6024	0.632
3.	10	18	250	75	18	0.7594	0.758
4.	10	18	275	80	19	0.9405	0.902
5.	10	18	300	85	20	1.1475	1.068
6.	10	19	200	70	18	0.5985	0.629
7.	10	19	225	75	19	0.7615	0.759
8.	10	19	250	80	20	0.9500	0.910
9.	10	19	275	85	16	0.8883	0.861
10.	10	19	300	65	17	0.7873	0.780
11.	10	20	200	75	20	0.7500	0.450
12.	10	20	225	80	16	0.7200	0.726
13.	10	20	250	85	17	0.9031	0.872
14.	10	20	275	65	18	0.8044	0.794
15.	10	20	300	70	19	0.9975	0.948
16.	10	21	200	80	17	0.7140	0.721
17.	10	21	225	85	18	0.9037	0.873
18.	10	21	250	65	19	0.8105	0.798
19.	10	21	275	70	20	1.0106	0.958
20.	10	21	300	75	16	0.9450	0.906
21.	10	22	200	85	19	0.8883	0.861
22.	10	22	225	65	20	0.8044	0.794
23.	10	22	250	70	16	0.7700	0.766
24.	10	22	275	75	17	0.9642	0.921
25.	10	22	300	80	18	1.1880	1.100
26.	20	18	200	65	19	0.8779	0.852
27.	20	18	225	70	20	1.1064	1.035
28.	20	18	250	75	16	1.3732	1.249
29.	20	18	275	80	17	1.6812	1.495
30.	20	18	300	85	18	2.0331	1.776
31.	20	19	200	70	16	1.0998	1.030
32.	20	19	225	75	17	1.3768	1.251
33.	20	19	250	80	18	1.6973	1.508
34.	20	19	275	85	19	1.5923	1.424
35.	20	19	300	65	20	1.4207	1.287
36.	20	20	200	75	18	1.3573	1.236
37.	20	20	225	80	19	1.3063	1.195
38.	20	20	250	85	20	1.6176	1.444
39.	20	20	275	65	16	1.4497	1.310
40.	20	20	300	70	17	1.7781	1.572
41.	20	21	200	80	20	1.2961	1.187
42.	20	21	225	85	16	1.6185	1.445
43.	20	21	250	65	17	1.4601	1.318
44.	20	21	275	70	18	1.8004	1.590
45.	20	21	300	75	19	1.6888	1.501
46.	20	22	200	85	17	1.5923	1.424
47.	20	22	225	65	18	1.4497	1.310
48.	20	22	250	70	19	1.3913	1.823
49.	20	22	275	75	20	1.7215	1.527
50.	20	22	300	80	16	2.1019	1.592
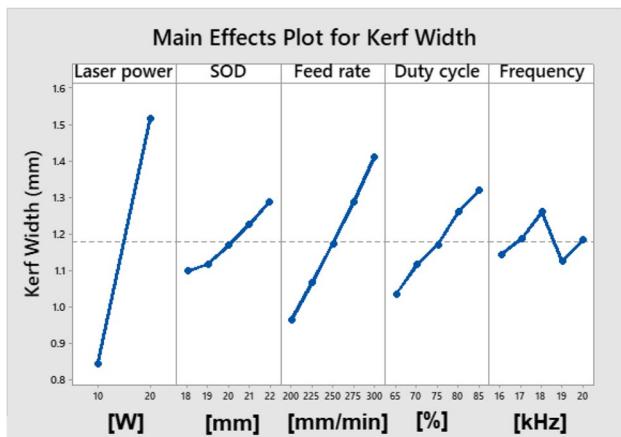
Fig. 6 Main effects plot of kerf width

Fig. 7 Main effects plot for surface roughness

Table 3 ANOVA results for kerf width

Source	DF	Adj SS	Adj MS	F-value	P-value
Regression	5	7.62817	1.52563	124.98	0.000
Laser power	1	5.65233	5.65233	463.06	0.000
SOD	1	0.23418	0.23418	19.18	0.000
Feed rate	1	1.23095	1.23095	100.84	0.000
Duty cycle	1	0.51041	0.51041	41.81	0.000
Frequency	1	0.00031	0.00031	0.03	0.874
Error	44	0.53709	0.01221		
Total	49	8.16526			

is proven to be statistically significant. This result is also confirmed based on the calculation of the delta factor in the results of the main effects plot by Taguchi analysis, as the most important parameter is proven to be laser power, whereas feed rate, duty cycle, SOD, and frequency have a smaller contribution to kerf width, accordingly.

3.1.2 Analysis of surface roughness values

Regarding surface roughness, it can be observed from Table 2 that the values of Ra vary between 0.450 and 1.823 µm during the DLBM experiments. Thus, it is possible that the choice of the appropriate values of the different process parameters can provide the desired surface roughness value. The results depicted in the main effects plot of Fig. 7 present the main trends occurring for the surface roughness values in respect to the process parameters.

Laser power is revealed to be again a dominant factor, as the increase of laser power between 10 and 20 W leads to a radical increase of surface roughness of the specimens in any case. Moreover, it is shown that the feed rate is also
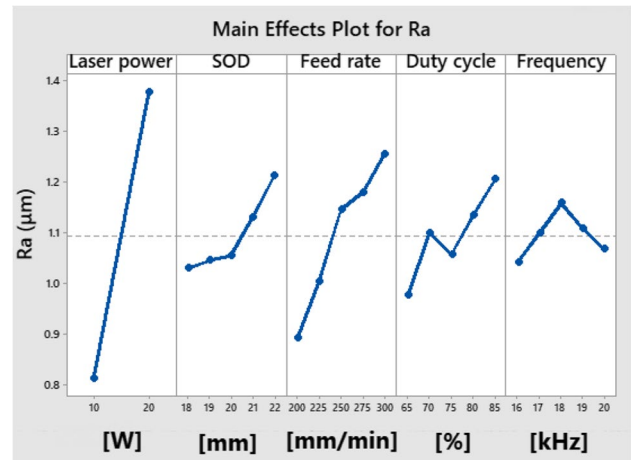
an important parameter for surface roughness given that it contributes to an almost linear increase of surface roughness. The duty cycle is another important parameter for regulating surface roughness, with a generally positive correlation with Ra, except for the range [70%, 80%] when a slight decrease of Ra was observed. Finally, SOD and frequency are the least important parameters with increased SOD resulting in a moderate increase of Ra and frequency leading to a slight increase of Ra up to 18 kHz and then to a slight decrease for values up to 20 kHz.

These trends can also be explained based on the specific characteristics of the laser beam machining process. When laser power is high, the more intense thermal phenomena such as melting and evaporation result in a rougher surface being developed. Moreover, the increase of duty cycle also contributes to a higher amount of energy being introduced to the workpiece leading to more radical alterations of surface topography, whereas the use of different frequencies seems to have a negligible effect on surface roughness as its variation is much lower than the variation induced by other parameters. Finally, in order to justify the importance of each parameter, in Table 4, the ANOVA results for surface roughness are depicted.

ANOVA results from Table 4 confirm the qualitative observations from the main effects plot for surface roughness as it is determined that all parameters except from frequency are statistically important for surface roughness, with laser power being the most important, followed by feed rate, duty cycle, and SOD. Thus, in order to achieve the desired surface roughness, it is important to choose appropriate values mainly for laser power, feed rate, and duty cycle. However, as it was stressed before, in practical applications, it is crucial to take into account multiple objectives, such as kerf width or MRR, as it will be performed in subsection 3.4.

3.1.3 Microscope observations of surface quality after DLBM

Finally, the experimental results prove the considerable potential of diode laser machining as the appropriate control of the process parameters can lead to the achievement of the desired kerf quality with sufficient precision. It was shown that the main parameters required to be varied for efficient regulation of kerf width are laser power and feed rate, as two of the main factors related to the heat input into the workpiece. However, the exact values of process parameters for efficient material removal by DLBM should be selected carefully in accordance with other performance metrics such as MRR, surface roughness, or power consumption, in order to be able to achieve not only high quality but also high productivity during DLBM of titanium alloys. Figure 8 shows SEM images of the bottom surfaces. Figure 8a is an image machined with 10-W laser power. It can be seen that the presence of pockmarks may be caused by the expulsion of molten

Table 4 ANOVA results for surface roughness

Source	DF	Adj SS	Adj MS	F-value	P-value
Regression	5	5.21672	1.04334	89.71	0.000
Laser power	1	3.95930	3.95930	340.42	0.000
SOD	1	0.20358	0.20358	17.50	0.000
Feed rate	1	0.80892	0.80892	69.55	0.000
Duty cycle	1	0.24157	0.24157	20.77	0.000
Frequency	1	0.00335	0.00335	0.29	0.594
Error	44	0.51174	0.01163		
Total	49	5.72846			

material or gas entrapment during the material's solidification. There is also the presence of microcracks caused by thermal stress due to the rapid heating and cooling during the laser milling process. On the other hand, in Fig. 8b, it is shown the bottom surface machined by 20-W laser power. This image has more rough surface with an intense presence of craters; these are depressions on the surface but might be larger and have a more defined edge. Craters can result from the impact of the laser pulse on the surface causing material removal. Additionally, there is a presence of globules which are spherical particles that have solidified on the surface. They could be remnants of molten material that cooled rapidly into spherical shapes due to surface tension.

3.2 Development of regression model

In order to gain further insight into the correlation of process parameters and kerf width, it is important to develop a regression model, which will take into account the obtained experimental results. Thus, after some preliminary investigations, a non-linear regression model was developed, including only the statistically significant terms, as follows:

$$K_W = 1.17661 * 10^{-6} LP^{0.843893} * SOD^{0.798317} \\ * FR^{0.936836} * DC^{0.921306} \tag{5}$$

This model has a MSE value of 0.0095629, RMSE value of 0.09779, MAPE value of 6.866%, and MAE value of 0.078629. The values of these metrics indicate that a sufficient level of correlation between process parameters and kerf width can be established through this model. However, it is also necessary to investigate further the possibility to
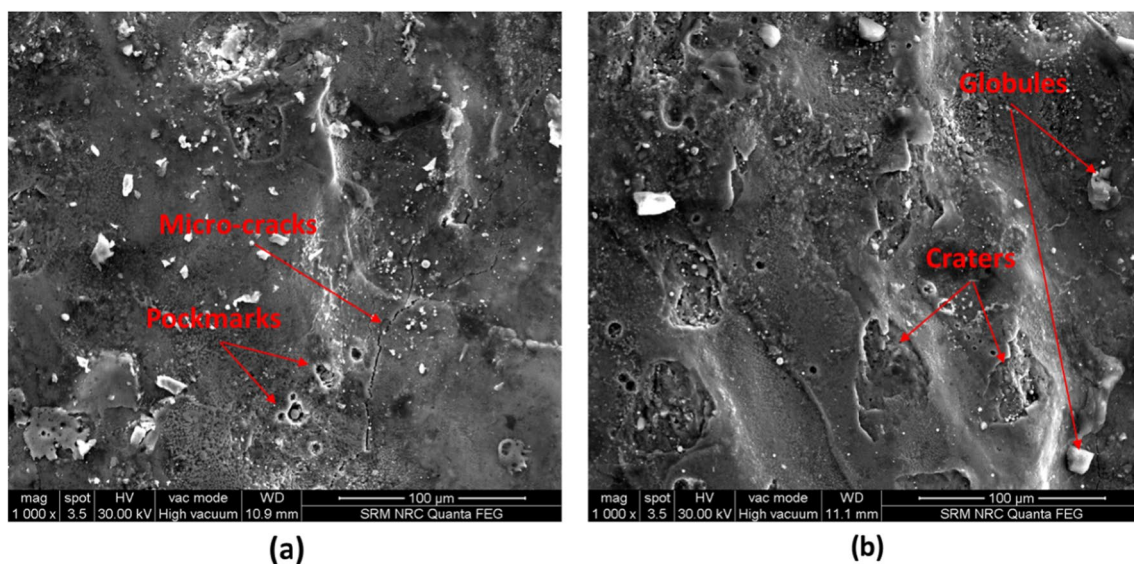

Fig. 8 SEM images that show surfaces machined by 10-W laser power (**a**) and by 20-W laser power (**b**)

develop a more precise and robust model based on AI techniques in order to be able to generalize more sufficiently and further reduce the errors.

3.3 Development of DT regression model

A relatively simple but useful machine learning (ML) model is decision tree (DT). This type of ML model not only is primarily effective for classification purposes but can also be used for regression. Especially, regression tree (RT) is an algorithm pertinent to the DT methods, which can be regarded as a supervised learning algorithm, able to handle both numerical and categorical values. The algorithm of RT is relatively simple, as it is partitioning the feature space in a recursive way, eventually creating smaller subsets based on the values of input parameters. Each node of the tree involves a splitting criterion in order to split the data into child nodes in the optimum way until the stopping criterion is true, e.g., maximum tree depth. The final model has a tree structure with the leaf nodes having the final predicted values of the target response based on specific values of the input parameters which lead to this node.

RT have various advantages such as direct interpretability, given that a visual representation of the tree structure can be obtained in order to under the function of the model and identify the most important features, handling of missing data, as the missing values are omitted during splitting, and establishment of non-linear correlations but they can suffer from overfitting, as most ML models, and they exhibit high computational costs due to large datasets.

The regression tree model developed in this work has a depth of four levels. The predictor importance estimated by the model is comparable to the results of ANOVA as the ranking of input variables was as follows: laser power, feed rate, duty factor, SOD, and frequency. Frequency had an importance value of 0 and was neglected in the RT model. The model was found to have a MSE value of 0.0148, RMSE value of 0.1216, MAPE value of 1.1741%, and MAE value of 0.0822. The values of these metrics indicate that the model was able to capture the correlation between input parameters and kerf width at a satisfactory level. However, compared to the non-linear regression model, MSE, RMSE, and MAE values are slightly higher but MAPE value was considerably decreased.
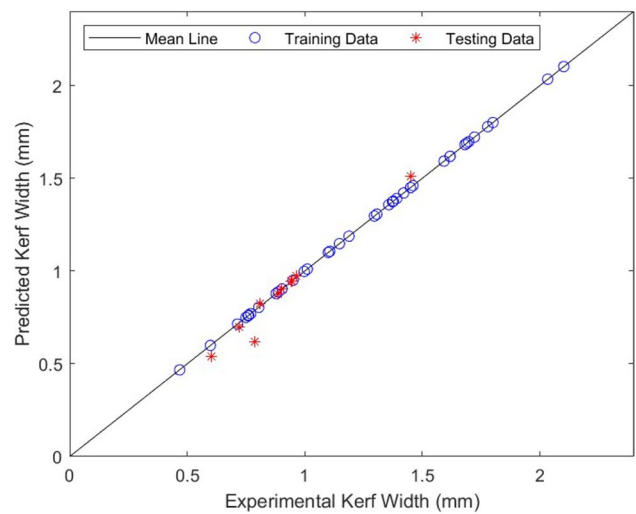

Fig. 9 Scatter diagram between measures and predicted values for both training and test data for ANFIS model

3.4 Performance of developed ANFIS model

There were in total 50 machining experiments that were conducted on titanium alloy specimens under various process variables' combinations, as shown in Table 2. The experimental values of K_W which are presented in Table 2 are utilized as the training data in ANFIS under the aforementioned machining settings, and the experimental dataset was randomly divided into training (40 numbers) and testing (10 numbers) datasets. The training dataset is used to train the predictive models and the testing dataset is used to validate the performance of the models. Training an ANFIS model involves adjusting its parameters to fit the training data. Since the aim of the study is to accurately predict K_W, ANFIS model is developed to estimate the K_W based on the input factors.

In an ANFIS structure, the input membership functions and rule base are tuned by ANN by an iterative learning process. ANFIS architecture and training parameters are shown in Table 5. So, the ANN tunes the fuzzy inference system to adapt to the input variables to accurately predict K_W. Figure 9 shows the scatter plot denoting the deviation from actual experimental K_W with the predicted values for both training and testing datasets. It is inferred from these results that the FIS is tuned

Table 5 ANFIS parameters

Number of nodes	524
Number of parameters	1503
Number of training dataset	40
Number of testing dataset	10
Number of fuzzy rules	243
Membership function	Bell
Fuzzy type	Sugeno

Table 6 GA parameters for tuning ANFIS

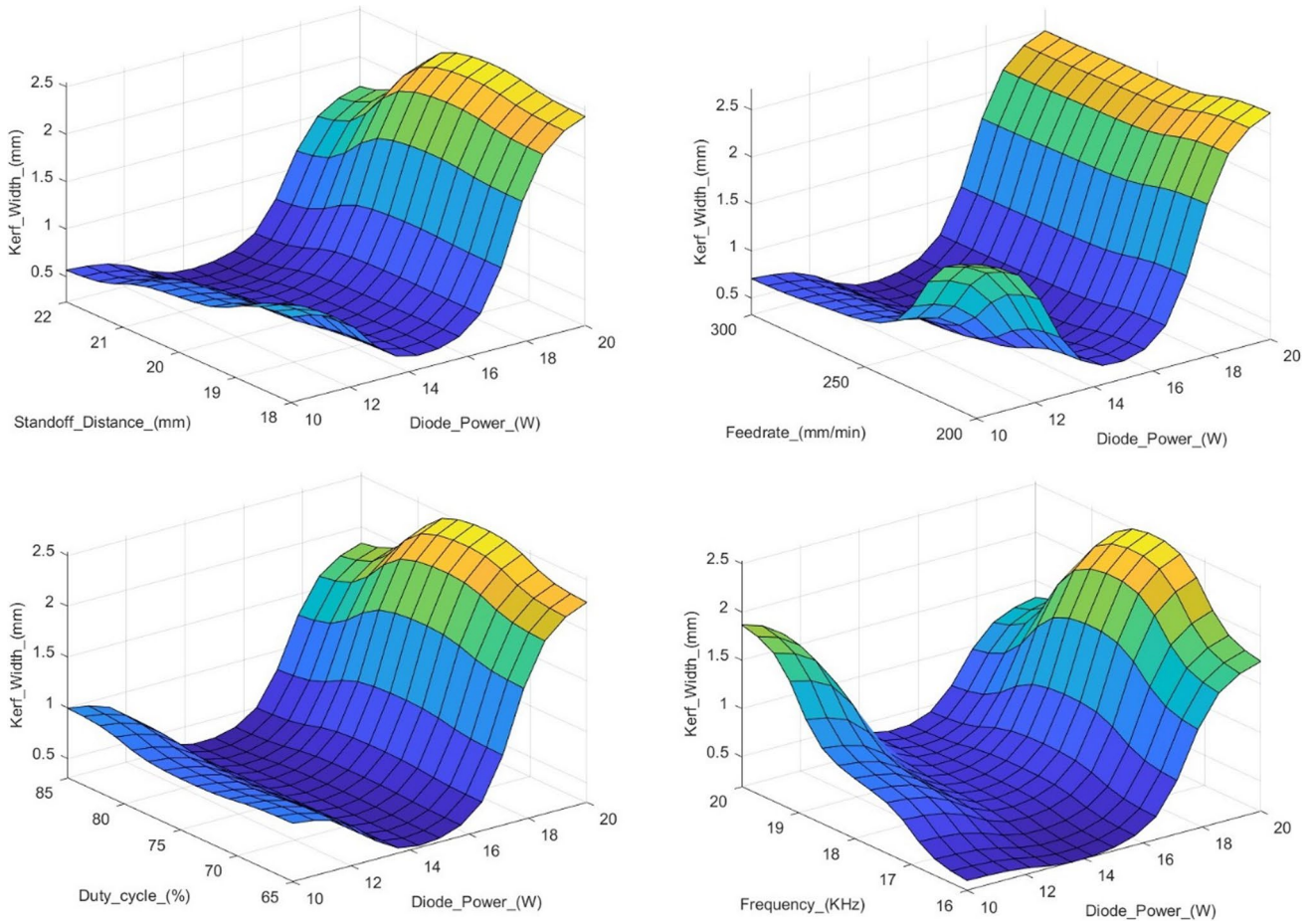|	
Population size	25
Maximum number of iterations	150
Crossover percentage	0.8
Mutation percentage	0.8
Mutation rate	0.001
Gamma	0.65

Fig. 10 Rule surfaces show relationship between input and output variables in the GA-ANFIS model

well using the ANN in the ANFIS model with an R^2 value of 0.99 for the training data but have only 0.94 value for the
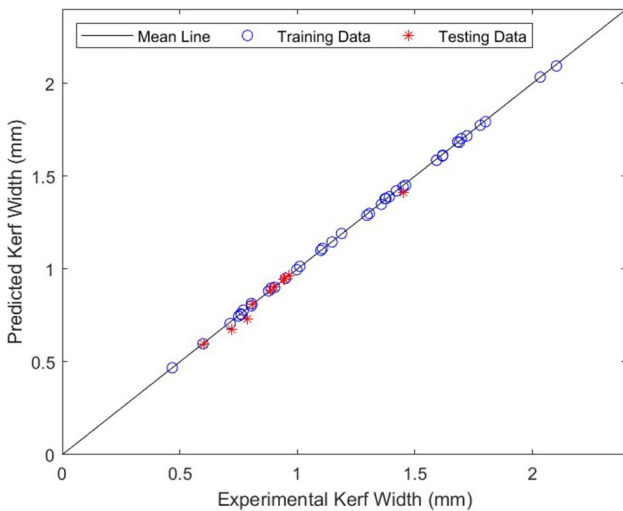

Fig. 11 Scatter diagram between measures and predicted values for both training and test data for the GA-ANFIS model

testing dataset. Also, the error parameters MSE, RMSE, and MAE are comparatively larger for the testing dataset compared to the training dataset. This is mainly due to the overfitting issue. This justifies the requirement of an additional algorithm to tune the ANFIS structure to improve the prediction results.

3.5 Performance of developed ANFIS model

Using a genetic algorithm (GA) to tune an adaptive neuro-fuzzy inference system (ANFIS) and then validating its performance is a powerful approach to achieve accurate and adaptable modeling for predicting kerf width. The ANFIS structure used in this model is similar as in Table 5 and the settings of GA parameters used to tune ANFIS are given in Table 6. The initial population of chromosomes with random parameter values is created. The crossover and mutation operations are applied to generate a new population of chromosomes. The iteration process repeats the selection, crossover, and mutation steps for a defined number of generations or until the convergence criterion is met. Thus, the GA-ANFIS model for predicting K_W has been developed.

Table 7 Performance comparison of ANFIS and GA-ANFIS models

Performance index	Training data		Testing data	
	ANFIS	GA-ANFIS	ANFIS	GA-ANFIS
MSE	0.000031	5.85094×10^{-08}	0.003694	0.000679
RMSE	0.005553	0.000241887	0.060778	0.026065
MAE	0.004720	9.43335×10^{-05}	0.035837	0.015658
R^2	0.99	0.99	0.94	0.98

Table 8 Performance comparison of GA-ANFIS models with standard regression models

Model	MSE	RMSE	MAE	R^2
Linear regression	0.008423	0.091778	0.066077	0.95
Non-linear regression	0.009563	0.097790	0.078629	0.94
Decision tree regression	0.014800	0.121600	0.082200	0.92
SVM	0.008898	0.094329	0.072205	0.95
Gaussian process regression	0.008586	0.092658	0.066470	0.95
Neural network	0.012346	0.111114	0.085391	0.93
Kernel regression	0.042897	0.207120	0.171918	0.89
GA-ANFIS	**0.000679**	**0.026065**	**0.015658**	**0.98**

The structure of the rule surfaces between the input and output variables for the GA-ANFIS model is shown in Fig. 10. Figure 11 shows the scatter plot denoting the deviation from actual experimental K_W with the predicted values for both training and testing datasets for the GA-ANFIS model.

The performance of GA-ANFIS is evaluated and compared with the ANFIS model using the performance measures such as MSE, RMSE, MAE, and coefficient of determination (R^2) as shown in Table 7. As per the results, it is evident that the predicting performance of the GA-ANFIS model is better with less value for error parameters (MSE, RMSE, MAE) and a higher R^2 value of 0.98. This makes
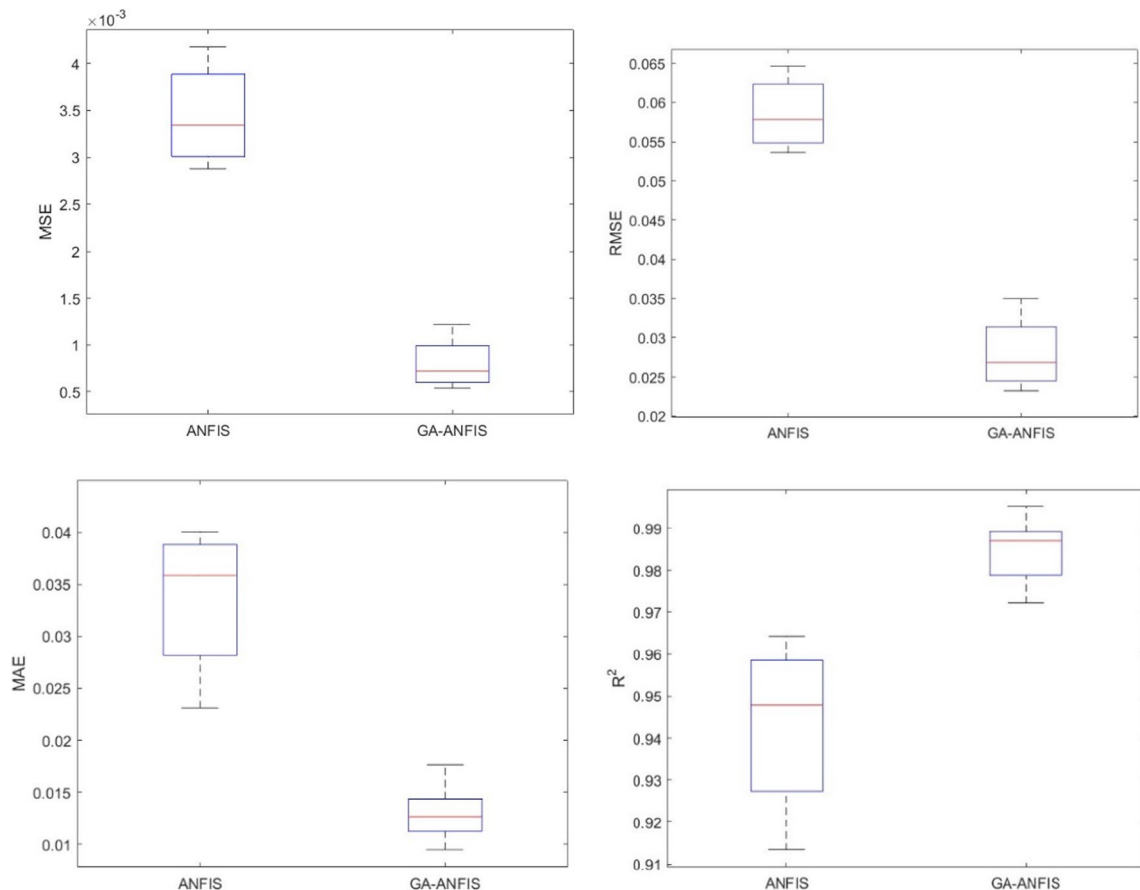

Fig. 12 Box plot of performance metrics for different prediction algorithms in different trials of 5-fold validation

Table 9 Performance comparison of ANFIS and GA-ANFIS models for different trails of 5-fold cross-validation

Trail no.	Model	MSE	RMSE	MAE	R^2
1	ANFIS	0.003791	0.061571	0.03584	0.93
	GA-ANFIS	0.000619	0.024880	0.01266	0.99
2	ANFIS	0.002874	0.053610	0.02312	0.96
	GA-ANFIS	0.001221	0.034943	0.01766	0.99
3	ANFIS	0.003342	0.057810	0.03842	0.91
	GA-ANFIS	0.000721	0.026851	0.00951	0.97
4	ANFIS	0.004180	0.064653	0.04005	0.95
	GA-ANFIS	0.000539	0.023216	0.01187	0.98
5	ANFIS	0.003051	0.055236	0.02988	0.96
	GA-ANFIS	0.000914	0.030232	0.01327	0.99

sure that there is no or less overfitting as the prediction accuracy for testing data is better as compared to training data. In comparison with the nonlinear regression model and the regression tree model, both ANFIS and GA-ANFIS exhibit superior MSE, RMSE, and MAE values.

The performance of developed GA-ANFIS was additionally compared with standard regressions models such as linear regression, support vector machine (SVM), multilayer perceptron neural network, Gaussian process regression, and kernel regression, apart from the regression models presented in subsections 3.2 and 3.3 in order to conduct a more comprehensive comparison with state-of-the-art models. These models are developed using MATLAB Regression Toolbox. Table 8 shows the performance comparison of the GA-ANFIS model with standard regression models for testing data. As the GA-ANFIS model exhibits less value for error parameters (MSE, RMSE, MAE) and a higher R^2 value, it can be inferred that it has better prediction characteristics.

3.6 Fivefold cross-validation of the GA-ANFIS model

Fivefold cross-validation is a technique used to assess the performance of the prediction model by dividing the dataset into five subsets or folds. The model is trained and evaluated five times, each time using a different fold as the validation set and the remaining folds as the training set. This method provides a more robust estimate of a model's generalization performance compared to a single train-test split. The dataset is randomly divided into five equal-sized subsets (folds). During each iteration, four folds are used for training, and the remaining fold is used for validation. Fivefold cross-validation provides a more reliable assessment of a model's performance compared to a single train-test split, as it accounts for potential variations in the data distribution. It reduces the risk of overfitting or underfitting on a particular dataset partition. Table 9 shows the performance comparison of ANFIS and GA-ANFIS models for different trials of fivefold cross-validation. A box plot, also known as

Fig. 13 Steps involved in GRB multi-response optimization

Calculation of S/N ratio:

- Smaller the better characteristics

$$\frac{S}{N} ratio = -10\log\frac{1}{m}\sum Y_{ni}^2$$

m - Number of experimental replications
Y_{ni} - Response of nth trial of ith dependent level.

Calculation of normalized S/N ratio:

- Smaller the better characteristics

$$Z_{ni} = \frac{\max\ (Y_{ni}) - Y_{ni}}{\max\ (Y_{ni}) - \ \min\ (Y_{ni})}$$

Z_{ni} - Normalized of nth trial of ith dependent level.

Computation of grey co-efficient (GC):

$$GC_{ni} = \frac{(\Psi_{min} + \delta\Psi_{max})}{(\Psi_{ni} + \delta\Psi_{max})}$$

Ψ_{ni}-Grey co-efficient for n^{th} trial of ith dependent response
δ -Distinctive co efficient which has value from 0 to 1

Computation of grey relation grade (G_n):

$$G_n = \frac{1}{Q}\sum GC_{ni}$$

q - Number of the performance measures

Table 10 *S/N* ratio and normalized *S/N* ratio arrays

Experiment no.	Kerf width		Surface roughness	
	S/*N* ratio	Normalized S/*N* ratio	S/*N* ratio	Normalized S/*N* ratio
1.	6.5951	0	5.6067	0.1114
2.	4.4023	0.1686	3.9868	0.2473
3.	2.3906	0.3233	2.4121	0.3793
4.	0.5328	0.4662	0.8920	0.5067
5.	−1.1951	0.5991	−0.5714	0.6294
6.	4.4587	0.1643	4.0297	0.2436
7.	2.3666	0.3252	2.3929	0.3809
8.	0.4455	0.4729	0.8192	0.5128
9.	1.0288	0.4281	1.3036	0.4722
10.	2.0772	0.3474	2.1599	0.4004
11.	2.4988	0.3150	6.9357	0.0000
12.	2.8534	0.2878	2.7813	0.3483
13.	0.8853	0.4391	1.1849	0.4822
14.	1.8906	0.3618	2.0088	0.4131
15.	0.0217	0.5055	0.4638	0.5426
16.	2.9260	0.2822	2.8389	0.3435
17.	0.8795	0.4395	1.1801	0.4826
18.	1.8249	0.3668	1.9556	0.4176
19.	−0.0916	0.5142	0.3683	0.5506
20.	0.4914	0.4694	0.8574	0.5096
21.	1.0288	0.4281	1.3036	0.4722
22.	1.8906	0.3618	2.0088	0.4131
23.	2.2702	0.3326	2.3154	0.3874
24.	0.3167	0.4828	0.7114	0.5219
25.	−1.4963	0.6223	−0.8310	0.6512
26.	1.1311	0.4202	1.3879	0.4651
27.	−0.8782	0.5747	−0.2998	0.6067
28.	−2.7547	0.7190	−1.9282	0.7432
29.	−4.5124	0.8542	−3.4926	0.8744
30.	−6.1632	0.9811	−4.9912	1.0000
31.	−0.8263	0.5707	−0.2554	0.6029
32.	−2.7774	0.7208	−1.9482	0.7449
33.	−4.5952	0.8606	−3.5671	0.8806
34.	−4.0405	0.8179	−3.0692	0.8389
35.	−3.0500	0.7417	−2.1886	0.7650
36.	−2.6535	0.7112	−1.8392	0.7357
37.	−2.3209	0.6857	−1.5476	0.7113
38.	−4.1774	0.8284	−3.1918	0.8491
39.	−3.2256	0.7552	−2.3438	0.7780
40.	−4.9991	0.8916	−3.9317	0.9112
41.	−2.2528	0.6804	−1.4881	0.7063
42.	−4.1823	0.8288	−3.1962	0.8495
43.	−3.2877	0.7600	−2.3988	0.7826
44.	−5.1074	0.9000	−4.0297	0.9194
45.	−4.5516	0.8572	−3.5278	0.8773
46.	−4.0405	0.8179	−3.0692	0.8389
47.	−3.2256	0.7552	−2.3438	0.7780
48.	−6.4083	1	−3.9569	0.9133
49.	−4.7181	0.8700	−3.6779	0.8899
50.	−5.1146	0.9005	−4.0362	0.9199

Table 11 Gray relational coefficient and gray relational grade for the present study

Experiment no.	Gray relational coefficient		Gray relational grade
	Kerf width	Surface roughness	
1.	0.3333	0.3601	0.3467
2.	0.3756	0.3991	0.3873
3.	0.4249	0.4461	0.4355
4.	0.4837	0.5034	0.4935
5.	0.5550	0.5743	0.5647
6.	0.3743	0.3980	0.3862
7.	0.4256	0.4468	0.4362
8.	0.4868	0.5065	0.4967
9.	0.4664	0.4865	0.4765
10.	0.4338	0.4547	0.4443
11.	0.4219	0.3333	0.3776
12.	0.4125	0.4342	0.4233
13.	0.4713	0.4912	0.4813
14.	0.4393	0.4600	0.4497
15.	0.5028	0.5223	0.5125
16.	0.4106	0.4323	0.4215
17.	0.4715	0.4914	0.4815
18.	0.4412	0.4619	0.4516
19.	0.5072	0.5267	0.5169
20.	0.4852	0.5049	0.4950
21.	0.4664	0.4865	0.4765
22.	0.4393	0.4600	0.4497
23.	0.4283	0.4494	0.4388
24.	0.4916	0.5112	0.5014
25.	0.5696	0.5891	0.5794
26.	0.4630	0.4832	0.4731
27.	0.5404	0.5597	0.5500
28.	0.6402	0.6607	0.6504
29.	0.7742	0.7992	0.7867
30.	0.9637	1.0000	0.9818
31.	0.5381	0.5574	0.5477
32.	0.6417	0.6621	0.6519
33.	0.7819	0.8072	0.7946
34.	0.7330	0.7563	0.7447
35.	0.6594	0.6803	0.6698
36.	0.6339	0.6542	0.6441
37.	0.6140	0.6339	0.6240
38.	0.7445	0.7682	0.7564
39.	0.6714	0.6926	0.6820
40.	0.8219	0.8491	0.8355
41.	0.6101	0.6300	0.6200
42.	0.7449	0.7686	0.7568
43.	0.6757	0.6970	0.6863
44.	0.8333	0.8612	0.8472
45.	0.7779	0.8030	0.7904
46.	0.7330	0.7563	0.7447
47.	0.6714	0.6926	0.6820
48.	1.0000	0.8522	0.9261
49.	0.7937	0.8195	0.8066
50.	0.8340	0.8620	0.8480

Table 12 Identification of optimal process parameters

Input factors	Average gray relational grade by parameter levels					Optimized parameters
	Level 1	Level 2	Level 3	Level 4	Level 5	
Laser power	0.4610	0.7240	N/A	N/A	N/A	20 W
Standoff distance	0.5670	0.5648	0.5786	0.6067	0.6453	22 mm
Feed rate	0.5038	0.5443	0.6118	0.6305	0.6721	300 mm/min
Duty cycle	0.5335	0.5948	0.5789	0.6088	0.6465	85%
Frequency	0.5665	0.5941	0.6282	0.5929	0.5808	18 kHz

a box-and-whisker plot, is a graphical representation that displays the distribution of a dataset. It shows the median, quartiles, and potential outliers of the data. In fivefold cross-validation, a box plot can help visualize the distribution of performance metrics MSE, RMSE, MAE, and R^2 across the different folds as shown in Fig. 12. The GA-ANFIS model has less variation of the performance metrics compared to the ANFIS model across different folds. It infers that GA-ANFIS for predicting kerf width model has less dependency on dataset, thus avoiding overfitting or underfitting issues.

3.7 Multi-response optimization of kerf width and surface roughness

In the present work, an attempt was made to adopt gray relational–based (GRB) multi-response optimization (MRO) for optimizing kerf width and surface roughness along with prediction of kerf width [58, 59]. The GRB approach can provide better accuracy among many MRO methods. The steps involved in GRB approach are explained in Fig. 13.

Both kerf width and surface roughness were considered as the smaller the better characteristics. The surface roughness of the cut surface was quantitatively measured using an Alicona Infinite focus microscope by setting up lambda filter (cut off wavelength) on 80 μm. Each machining trial was replicated two times to enhance the measurement accuracy and all the performance characteristic values used for analysis was obtained from computing the mean values of the repeated trials. The surface roughness was measured from scanned areas at the centre of the machined surface [60]. Table 10 shows the *S/N* ratio and normalized *S/N* ratio of the performance measures. Table 11 depicts the gray relational coefficient of all the experiments conducted.

The average gray relational grade on all levels of significant factors shows that the overall effect of responses in the machining process is as shown in Table 12. Therefore, average gray relational grade analysis was utilized to obtain the most optimum combination of process parameters on all levels. It was noted the highest average gray relational grade as 20 W (level 2) for laser power, 22 mm (level 5) for standoff distance, 300 mm/min (level 5) for feed rate, 85% (level 5) for duty cycle, and 18 kHz (level 3) for frequency.

The confirmation tests were carried out to ensure the accuracy of the optimal process parameters and optimization algorithm. In the confirmation experiment, the machining trial has been conducted with the computed optimum machining parameters and the responses have been analyzed. The estimated gray relational grade can provide an expected value of gray relational grade after the confirmation test [61]. It is used to statistically determine the amount of improvement that can be expected by machining the material surface with the optimized machining parameter combination. The estimated gray relational grade (G_p) for the optimum level of process parameters is computed from Eq. 6.

$$G_p = G_m + \sum (G_i - G_m) \tag{6}$$

Where G_m denotes the mean of the overall gray relational grade and G_i denotes the mean of the gray relational grade for each process parameter on its optimum level. The gray relational grade has been improved by 4.59% from the gray relational grade for the optimized parameters.

4 Conclusion

In this investigation, an endeavor was made to introduce the GA-tuned ANFIS technique to predict kerf width while machining grooves in a titanium alloy workpiece using the DLBM process and use gray relational–based optimization approach in order to determine the optimum process parameters for minimizing both kerf width and surface roughness. After the experimental results were analyzed by appropriate statistical techniques, the ANFIS model and GA-tuned ANFIS model were validated by comparing values from prediction and experiments for analyzing the accuracy of models and the GRB method leading to the optimum parameters for improving part quality. The following conclusions were made based on the observations:

- The analysis of the experimental results revealed that laser power plays the most significant role regarding kerf width, followed by feed rate, duty factor, and SOD, whereas frequency is not statistically significant. Moreover, similar conclusions were also drawn regarding surface roughness, with laser power being again identified as the dominant parameter for regulating surface quality.
- Non-linear regression model and regression tree model can provide a sufficient level of accuracy for the pre-

diction of kerf width with the former exhibiting lower MSE, RMSE, and MAE values, whereas the latter exhibits its lower MAPE.

- The FIS was effectively fine-tuned using an artificial neural network (ANN) within the ANFIS model, yielding an impressive R^2 value of 0.99 during training. However, this strong performance might suggest overfitting, as the R^2 value dropped to 0.94 when tested on an independent dataset.
- The predicting performance of the GA-ANFIS model was better with less value for error parameters (MSE, RMSE, MAE) and a higher R^2 value of 0.98. This infers that the problem of overfitting is reduced significantly by usage of genetic algorithm. Moreover, both of these networks outperform the non-linear regression and regression tree models.
- Additional comparison of the proposed GA-ANFIS models with various regression models such as linear regression, SVM, Gaussian process regression, multilayer perceptron neural network, and kernel regression proved that this model outperforms every other model in terms of MSE, RMSE, MAE, and R^2.
- In the fivefold cross-validation, the GA-ANFIS model has less variation of the performance metrics compared to the ANFIS model across different folds. This implies the dependency of the prediction model on the training data is reduced significantly by usage of genetic algorithm.
- The optimal process parameters were found as 20 W (level 2) for laser power, 22 mm (level 5) for standoff distance, 300 mm/min (level 5) for feed rate, 85% (level 5) for duty cycle, and 18 kHz (level 3) for frequency.

Finally, it should be noted that it is planned to improve the prediction accuracy by implementing deep neural networks and other advanced machine learning algorithms in future as well as developing real-time online prediction and preventive control system for the DLBM process.

Declarations

References

1. Nikolidakis E, Antoniadis A (2019) FEM modeling simulation of laser engraving. Int J AdvManufTechnol 105:3489–3498. https://doi.org/10.1007/s00170-019-04603-3
2. Auwal ST, Ramesh S, Yusof F et al (2018) A review on laser beam welding of titanium alloys. Int J AdvManufTechnol 97:1071–1098. https://doi.org/10.1007/s00170-018-2030-x
3. Singh T, Arab J, Chen S-C (2023) Improvement on surface quality of Inconel-718 slits via laser cutting and wire electrochemical machining processes. Opt Laser Technol 167:109637. https://doi.org/10.1016/j.optlastec.2023.109637
4. Kr Avanish, Dubey VinodYadava (2008) Experimental study of Nd:YAG laser beam machining—an overview. J Mater Process Technol 195(1–3):15–26. https://doi.org/10.1016/j.jmatprotec.2007.05.041
5. Muthuramalingam T, Moiduddin K, Akash R, Syed Krishnan S, HammadMian WadeaAmeen, HishamAlkhalefah, (2020) Influence of process parameters on dimensional accuracy of machined titanium (Ti-6Al-4V) alloy in Laser Beam Machining Process. Opt Laser Technol 132:106494. https://doi.org/10.1016/j.optlastec.2020.106494. https://doi.org/10.1016/j.optlastec.2020.106494
6. El-Hofy MH, El-Hofy H (2019) Laser beam machining of carbon fiber reinforced composites: a review. Int J AdvManufTechnol 101:2965–2975. https://doi.org/10.1007/s00170-018-2978-6
7. Ali NaderiBakhtiyari Z, Wang L, Wang, HongyuZheng (2021) A review on applications of artificial intelligence in modeling and optimization of laser beam machining. Opt Laser Technol. https://doi.org/10.1016/j.optlastec.2020.106721. (135, 2021, 106721, ISSN 0030-3992)
8. Parandoush P, Hossain A (2014) A review of modeling and simulation of laser beam machining. Int J Mach Tools Manuf 85:135–145. https://doi.org/10.1016/j.ijmachtools.2014.05.008
9. Ouyang Z, Long J, Wu J, Lin J, Xie X, Tan G, Yi X (2022) Preparation of high-quality three-dimensional microstructures on polymethyl methacrylate surfaces by femtosecond laser micromachining and thermal-induced micro-leveling. Opt Laser Technol
10. Marimuthu S, Dunleavey J, Liu Y, Antar M, Smith B (2019) Laser cutting of aluminium-alumina metal matrix composite. Opt Laser Technol 117. https://doi.org/10.1016/j.optlastec.2019.04.029
11. Meijer J (2004) Laser beam machining (LBM), state of the art and new opportunities. J Mater Process Technol 149(1–3):2–17. https://doi.org/10.1016/j.jmatprotec.2004.02.003
12. Yi Shi Z, Jiang J, Cao, Kornel F, Ehmann (2020) Texturing of metallic surfaces for superhydrophobicity by water jet guided laser micro-machining. Appl Surf Sci 500:0169–4332. https://doi.org/10.1016/j.apsusc.2019.144286
13. Karaboga D, Kaya E (2019) Adaptive network based fuzzy inference system (ANFIS) training approaches: a comprehensive survey. ArtifIntell Rev 52:2263–2293. https://doi.org/10.1007/s10462-017-9610-2
14. Golafshani EM, Behnood A, Arashpour M (2020) Predicting the compressive strength of normal and high-performance concretes using ANN and ANFIS hybridized with grey wolf optimizer. Construction and Building Materials 232:117266. https://doi.org/10.1016/j.conbuildmat.2019.117266
15. Anh TH, SandroNižetić Ong, Van Pham WT, Le Tri Hieu, QuangChau Minh, Nguyen Xuan Phuong (2021) A review on application of artificial neural network (ANN) for performance and emission characteristics of diesel engine fueled with biodiesel-based fuels. Sustain Energy Technol Assess 47:101416. https://doi.org/10.1016/j.seta.2021.101416
16. Senthilselvi A, Duela JS, Prabavathi R et al (2021) Performance evaluation of adaptive neuro fuzzy system (ANFIS) over fuzzy

inference system (FIS) with optimization algorithm in de-noising of images from salt and pepper noise. J Ambient Intell Hum Comput. https://doi.org/10.1007/s12652-021-03024-z

17. Mengyao Pang J, Li HM, Al-Tamimi DH, Elkamchouchi JJ, Ponnore H, Elhosiny Ali (2023) Development of hybrid ANFIS-GAN-XGBOOST models for accurate prediction of material removal rates from PCB-polluted concrete surfaces using laser technology for sustainable energy generation. Adv Eng Softw 184(103500):0965–9978. https://doi.org/10.1016/j.advengsoft.2023.103500

18. Viktor Molnar, GergelySzabo (2022) Designation of minimum measurement area for the evaluation of 3D surface texture. J Manuf Process 83. https://doi.org/10.1016/j.jmapro.2022.08.042

19. Ghazi Alsoruji T, Muthuramalingam Essam B, Moustafa Ammar Elsheikh (2022) Investigation and TGRA based optimization of laser beam drilling process during machining of Nickel Inconel 718 alloy. J Mater Res Technol 18:720–730. https://doi.org/10.1016/j.jmrt.2022.02.112

20. Chatterjee S, Mahapatra SS, Bharadwaj V et al (2021) Prediction of quality characteristics of laser drilled holes using artificial intelligence techniques. Engineering with Computers 37:1181–1204. https://doi.org/10.1007/s00366-019-00878-y

21. Eltawahni HA, Benyounis KY, Olabi AG (2016) High power CO2 laser cutting for advanced materials – review, Reference Module in Materials Science and Materials Engineering, Elsevier, ISBN 9780128035818, https://doi.org/10.1016/B978-0-12-803581-8.04019-4

22. Campanelli SL, Casalino G, Ludovico AD et al (2013) An artificial neural network approach for the control of the laser milling process. Int J AdvManufTechnol 66:1777–1784. https://doi.org/10.1007/s00170-012-4457-9

23. Rajamani D, Siva Kumar M, Balasubramanian E, Tamilarasan A (2021) Nd: YAG laser cutting of Hastelloy C276: ANFIS modeling and optimization through WOA. Mater Manuf Processes 36(15):1746–1760. https://doi.org/10.1080/10426914.2021.1942910

24. NaderiBakhtiyari Ali, Yongling Wu, Qi Dongfeng, HongyuZheng (2023) Modeling temporal and spatial evolutions of laser-induced plasma characteristics by using machine learning algorithms. Optik 272:170297. https://doi.org/10.1016/j.ijleo.2022.170297

25. Vasanth S, Muthuramalingam T, Prakash SS, Raghav SS, Logeshwaran G (2023) Experimental Investigation of PWM laser standoff distance control for power diode based LBM. Opt Laser Technol 158:108916

26. Vasanth S, Muthuramalingam T (2021) Application of laser power diode on leather cutting and optimization for better environmental quality measures. Archives Civil Mech Eng 21(2):54

27. Vasanth S, Muthuramalingam T, Prakash SS, SRaghav S (2023) Investigation of SOD control on leather carbonization in diode laser cutting. Mater Manuf Processes 38(5):544–553

28. Löhr C, Fé-Perdomo IL, Ramos-Grez JA, Calvo J (2021) Kerf profile analysis and neural network-based modeling of increasing thickness PMMA sheets cut by CO_2 laser. Opt Laser Technol 144:107386

29. Pramanik D, Goswami S, Kuar AS, Sarkar S, Mitra S (2019) A parametric study of kerf deviation in fiber laser micro cutting on Ti6Al4V superalloy. Mater Today: Proc 18(7):3348–3356

30. Pramanik D, Kuar AS, Sarkar S, Mitra S (2020) Optimization of edge quality on stainless steel 316L using low power fibre laser beam machining. Adv Mater Process Technol 7(1):42–53

31. Son S, Lee D (2020) The effect of laser parameters on cutting metallic materials. Materials 13(20):4596

32. Sakthivel G, Saravanakumar D, Muthuramalingam T (2018) Application of failure mode and effects analysis in manufacturing industry- an integrated approach with FAHP - FUZZY TOPSIS and FAHP -FUZZY VIKOR. Int J Productivity Qual Manage 24(3):398–423

33. Genna S, Menna E, Rubino G, Tagliaferri V (2020) Experimental investigation of industrial laser cutting: the effect of the material selection and the process parameters on the kerf quality. Appl Sci 10(14):4956

34. Lind J, Hagenlocher C, Weckenmann N, Blazquez-Sanchez D, Weber R, Graf T (2023) Adjustment of the geometries of the cutting front and the kerf by means of beam shaping to maximize the speed of laser cutting. Int J Adv Manuf Technol 126:1527–1538

35. Kusuma AI, Huang Y-M (2022) Performance comparison of machine learning models for kerf width prediction in pulsed laser cutting. Int J Adv Manuf Technol 123:2703–2718

36. Khoshaim Ahmed B, Elsheikh Ammar H, Moustafa Essam B, Basha Muhammad, Showaib Ezzat A (2021) Experimental investigation on laser cutting of PMMA sheets: effects of process factors on kerf characteristics. Journal of Materials Research and Technology 11:235–246

37. Zhipeng Pan Y, Feng T-P, Hung Y-C, Jiang F-C, Hsu L-T, Wu C-F, Lin Y-C, Lu, Steven Y, Liang (2017) Heat affected zone in the laser-assisted milling of Inconel 718. J Manuf Process 30:141–147

38. Feng Y, Hung TP, Lu YT et al (2019) Analytical prediction of temperature in laser-assisted milling with laser preheating and machining effects. Int J AdvManufTechnol 100:3185–3195

39. Elsheikh AH, Muthuramalingam T, Elaziz MA, Ibrahim AMM, Showaib EA (2022) Minimization of fume emissions in laser cutting of polyvinylchloride sheets using genetic algorithm. Int J Environ Sci Technol 19(7):6331–6344

40. Muthuramalingam T, Akash R, Krishnan S, HuuPhan N, Pi VN, Elsheikh AH (2021) Surface quality measures analysis and optimization on machining titanium alloy using CO2 based laser beam drilling process. J Manuf Process 62:1–6

41. Mohamed Rabik M, Vasanth S, Muthuramalingam T (2024) Implementation of LQR based SOD control in diode laser beam machining on leather specimens. Opt Laser Technol 170:110328

42. Khalaf T, Muthuramalingam T, Moiduddin K, Swaminathan V, Mian SH, Ahmed F, Aboudaif MK (2023) Performance evaluation of input power of diode laser on machined leather specimen in laser beam cutting process. Materials 16(6):2416

43. Saravanakumar D, Sakthivel G, Jegadeeshwaran R, Pathi JL, Kumar MM, Muthuramalingam T (2022) Assessment of vehicle handling performance of drivers using machine learning algorithms. IEEE Access 10:132288–132297

44. Bobzin K, Heinemann H, &Dokhanchi SR (2023) Development of an expert system for prediction of deposition efficiency in plasma spraying. J Therm Spray Tech 32:643–656. https://doi.org/10.1007/s11666-022-01494-x

45. Armaghani DJ, Asteris PG (2021) A comparative study of ANN and ANFIS models for the prediction of cement-based mortar materials compressive strength. Neural Comput&Applic 33:4501–4532. https://doi.org/10.1007/s00521-020-05244-4

46. Muthuramalingam T, Saravanakumar D, Babu LG et al (2020) Experimental investigation of white layer thickness on EDM processed silicon steel using ANFIS approach. Silicon 12:1905–1911. https://doi.org/10.1007/s12633-019-00287-2

47. Ji M, Muthuramalingam T, Saravanakumar D, Obratański PK, Karkalos NE, Zhang W (2023) Predicting depth of cut in vibration-assisted EDM cutting on titanium alloy using adaptive neuro fuzzy inference system. Measurement 219:113245. https://doi.org/10.1016/j.measurement.2023.113245

48. Zhou J, Li C, Arslan CA et al (2021) Performance evaluation of hybrid FFA-ANFIS and GA-ANFIS models to predict particle size distribution of a muck-pile after blasting. Engineering with Computers 37:265–274. https://doi.org/10.1007/s00366-019-00822-0

49. Zanaganeh M, Mousavi SJ, Shahidi AFE (2009) A hybrid genetic algorithm–adaptive network-based fuzzy inference system in prediction of wave parameters. Eng Appl Artif Intell 22(8):1194–1202. https://doi.org/10.1016/j.engappai.2009.04.009

50. Ghorbanzadeh O, Rostamzadeh H, Blaschke T et al (2018) A new GIS-based data mining technique using an adaptive neuro-fuzzy inference system (ANFIS) and k-fold cross-validation approach for land subsidence susceptibility mapping. Nat Hazards 94:497–517. https://doi.org/10.1007/s11069-018-3449-y

51. Singh NK, Singh Y, Kumar S et al (2020) Integration of GA and neuro-fuzzy approaches for the predictive analysis of gas-assisted EDM responses. SN Appl Sci 2:137. https://doi.org/10.1007/s42452-019-1533-x

52. Liu Y, Zhang S, Zhao Y, Ren Z (2022) Experiments on the kerf quality characteristic of mild steel while cutting with a high-power fiber laser. Opt Laser Technol 154:108332

53. Rao KV, Raju LS, Suresh G, Ranganayakulu J, Krishna J (2024) Modeling of kerf width and surface roughness using vibration signals in laser beam machining of stainless steel using design of experiments. Opt Laser Technol 169:110146

54. Darwish S, Ahmed N, Alahmari AM, Mufti NA (2016) A comparison of laser beam machining of micro-channels under dry and wet mediums. Int J Adv Manuf Technol 83:1539–1555

55. Kondayya D, Krishna AG (2013) An integrated evolutionary approach for modelling and optimization of laser beam cutting process. Int J Adv Manuf Technol 65:259–274

56. Lind J, Fetzer F, Blazquez-Sanchez D, Weidensdörfer J, Weber R, Graf T (2020) Geometry and absorptance of the cutting fronts during laser beam cutting. J Laser Appl 32:032015

57. Vasanth S, Muthuramalingam T (2022) Measurement of carbonization region on leather cutting in CO_2 and diode laser-based laser beam process. Proc Inst Mech Eng, Part E 236(3):1076–1082. https://doi.org/10.1177/09544089211056317

58. Ghazi Srouhgi T, Muthuramalingam, Essam B, Moustafa AE (2022) Investigation and TGRA based optimization of laser beam drilling process during machining of Nickel Inconel 718 alloy. J Mater Res Technol 18:720–730

59. Nguyen HuuPhan BT, AqibMashood LK, DucQuy T, Van Dong P, Muthuramalingam T, DucToan N (2020) Application of TGRA-based optimisation for machinability of high-chromium tool steel in the EDM process. Arab J Sci Eng 45(7):5555–5562

60. Muthuramalingam T (2019) Effect of diluted dielectric medium on spark energy in green EDM process using TGRA approach. J Clean Prod 238:117894

61. Jayakrishnan U, IkshitSanghrajka S, Manikandakumar T, Muthuramalingam M, Goldberg G, Littlefair (2018) Optimisation of multiple response characteristics on end milling of aluminium alloy using Taguchi-grey relational approach. Measurement 124:291–298